Available online at www.sciencedirect.com

ScienceDirect

Ceramics International 41 (2015) 13189–13200

CERAMICS INTERNATIONAL

www.elsevier.com/locate/ceramint

Multiferroic (NiZn) Fe_2O_4–$BaTiO_3$ composites prepared from nanopowders by auto-combustion method

A.S. Dzunuzovic[a], M.M.Vijatovic Petrovic[a], B.S. Stojadinovic[b], N.I. Ilic[a], J.D. Bobic[a], C.R. Foschini[c], M.A. Zaghete[d], B.D. Stojanovic[a,*]

[a]Institute for Multidisciplinary Research University of Belgrade, Belgrade, Serbia
[b]Institute of Physics, University of Belgrade, Serbia
[c]UNESP, Faculty for Engineering, Bauru, SP, Brazil
[d]UNESP, Institute for Chemistry, Araraquara, SP, Brazil

Received 24 June 2015; received in revised form 10 July 2015; accepted 16 July 2015
Available online 4 August 2015

Abstract

Nickel zinc ferrite (NZF) and barium titanate (BT) were prepared by auto-combustion synthesis as an effective, simple and rapid method. Multiferroic composites with the general formula $yNi_{1-x}Zn_xFe_2O_4-(1-y)$BT ($x=0.3$, 0.5, 0.7, $y=0.5$) were prepared by mixing NZF and BT powders in a liquid medium in the ball mill. The FEG micrographs indicated the primary particle size less than 100 nm for both, barium titanate and nickel zinc ferrite phases. X-ray analysis and Raman spectroscopy indicated the formation of well crystallized structure of NZF and BT phase in the composite powders and ceramics, with a small contribution of the secondary phase. The homogenous phase distribution in obtained composites was also confirmed. Impedance spectroscopy measurements were carried out in order to investigate the electrical resistivity of materials, showing that grain boundaries have greater impact on the total resistivity than grains. Saturation magnetization and remnant magnetization continuously decrease with barium titanate phase increase.

Keywords: A. Powders: chemical preparation; B. Composites; C. Impedance; D. $BaTiO_3$ and titanates; D. Ferrites

1. Introduction

Miniaturization of the solid-state electronics is achieved by downscaling and multifunctionality. Ferroics and multiferroics are among the most attractive multifunctional materials [1]. These nanostructured materials stimulated a sharply increasing interest to their significant technological promise in novel devices due to fact that the combination of dissimilar materials in ferroic-based oxide nanocomposites resulted in totally novel functionality.

The term multiferroic (MF) was first used by Schmid in 1994. His definition referred to multiferroics as a single phase materials which simultaneously possess two or more primary ferroic (ferroelectric, ferromagnetic and ferroelastic) properties. Today the term multiferroic has been expanded to include materials which exhibit any type of long range magnetic ordering, spontaneous electric polarization, and/or ferroelasticity. Working under this expanded definition the history of magnetoelectric multiferroics can be traced back to the 1960s [1–3]. In the most general sense the field of multiferroics was born from studies of magnetoelectric systems [4–6]. After an initial burst of interest, research remained static until early 2000. In 2003 the discovery of large ferroelectric polarization in epitaxially grown thin films of $BiFeO_3$ [7] and the discovery of strong magnetic and electric coupling in orthorhombic $TbMnO_3$ and $TbMn_2O_5$ have stimulated activity in the field of multiferroics. Besides scientific interest in their physical properties, multiferroics are interesting due to their potential applications as transducers, actuators, switches, magnetic field

*Corresponding author.
E-mail address: bstojanovic80@yahoo.com (B.S. Stojadinovic).

http://dx.doi.org/10.1016/j.ceramint.2015.07.096
0272-8842/

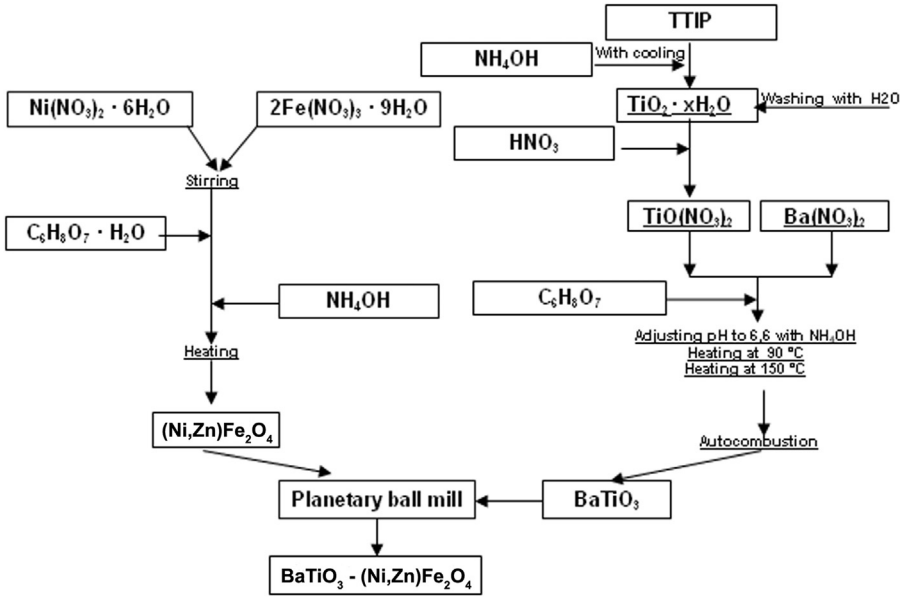

Fig. 1. Scheme of NZF, BT and composites preparation.

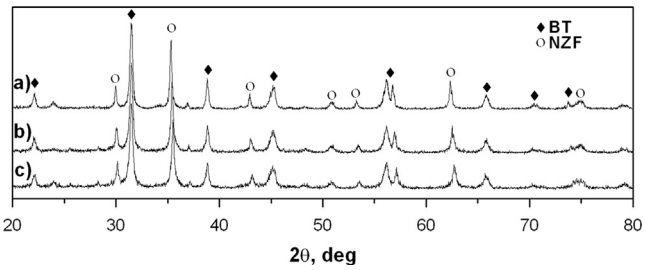

Fig. 2. The X-ray diffraction patterns of (a) NZF(30–70)−BT, (b) NZF(50–50)−BT and (c) NZF(70–30)–BT powders.

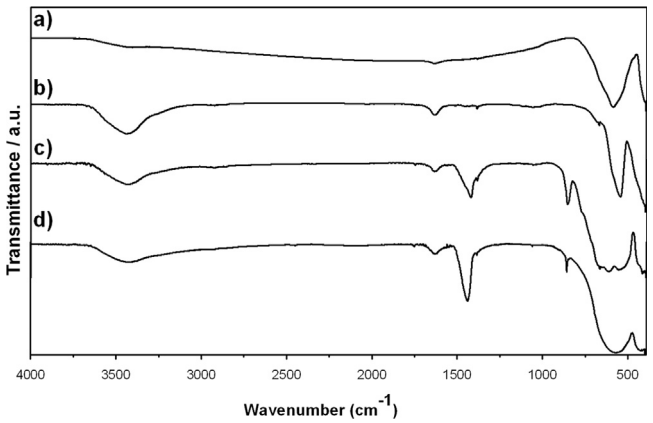

Fig. 3. FT-IR spectra of (a) NF, (b) ZF, (c) BT and (d) NZF(70–30)−BT powders.

sensors, new types of electronic memory devices, capacitive/inductive passive filters for telecommunications, etc. [8,9]. A large number of publications have been dedicated to multiferroics, dealing with theoretical, experimental, and application aspects [2,10]. In spite of hundreds of publications focused to single or composite multiferroic materials in the last years, they remain highly controversial concerning their preparation methods, phase stability, intrinsic polarization and switching, ferroelectric, ferromagnetic and magnetoelectric properties, etc. [10].

Multiferroic properties can appear in a large variety of materials [11]. The ferroelectric–ferromagnetic composites, as two-phase multiferroic materials, are desired not only for the fundamental research of magneto-electric effect, but also for the potential applications in many electronic devices [12]. The most widely studied systems correspond to Co or Ni ferrites, with PZT, PNT, BT or BST [13]. Among them, the Ni–Zn ferrites/$BaTiO_3$ systems need to be further investigated because of high electrical resistivity, chemical stability and excellent electromagnetic properties of the Ni–Zn ferrites, and high permittivity, low dielectric loss and high tunability of $BaTiO_3$ [4–6]. Those composites have attracted considerable attention as a new class of nanoferrites, expanding their use in other areas, such as drug delivery, heterogeneous catalysis, levitated railway system, magnetic-refrigeration, microwave devices, antennas, etc. [14].

To obtain the multiferroics, several routes for conventional material fabrication are being applied. Popular techniques within the multiferroic community are: solid state synthesis, hydrothermal synthesis, sol–gel processing, vacuum based deposition or other wet chemical synthesis methods. However, some types of multiferroics require specific processing conditions within more appropriate techniques. Consequently, multiferroic composites request methods for the synthesis both components: ferroelectric and ferromagnetic.

Ferrites crystallize in three crystal type: spinel, garnet type and magnetoplumbite type [15,16]. Meanwhile, the main attention is stressed to spinel type of ferrites that can be synthesized by a sol–gel method, conventional solid state reaction, mechanical attrition, hydrothermal synthesis, self-propagating combustion method, thermolysis, wet chemical co-precipitation technique, self-propagating, microemulsion,

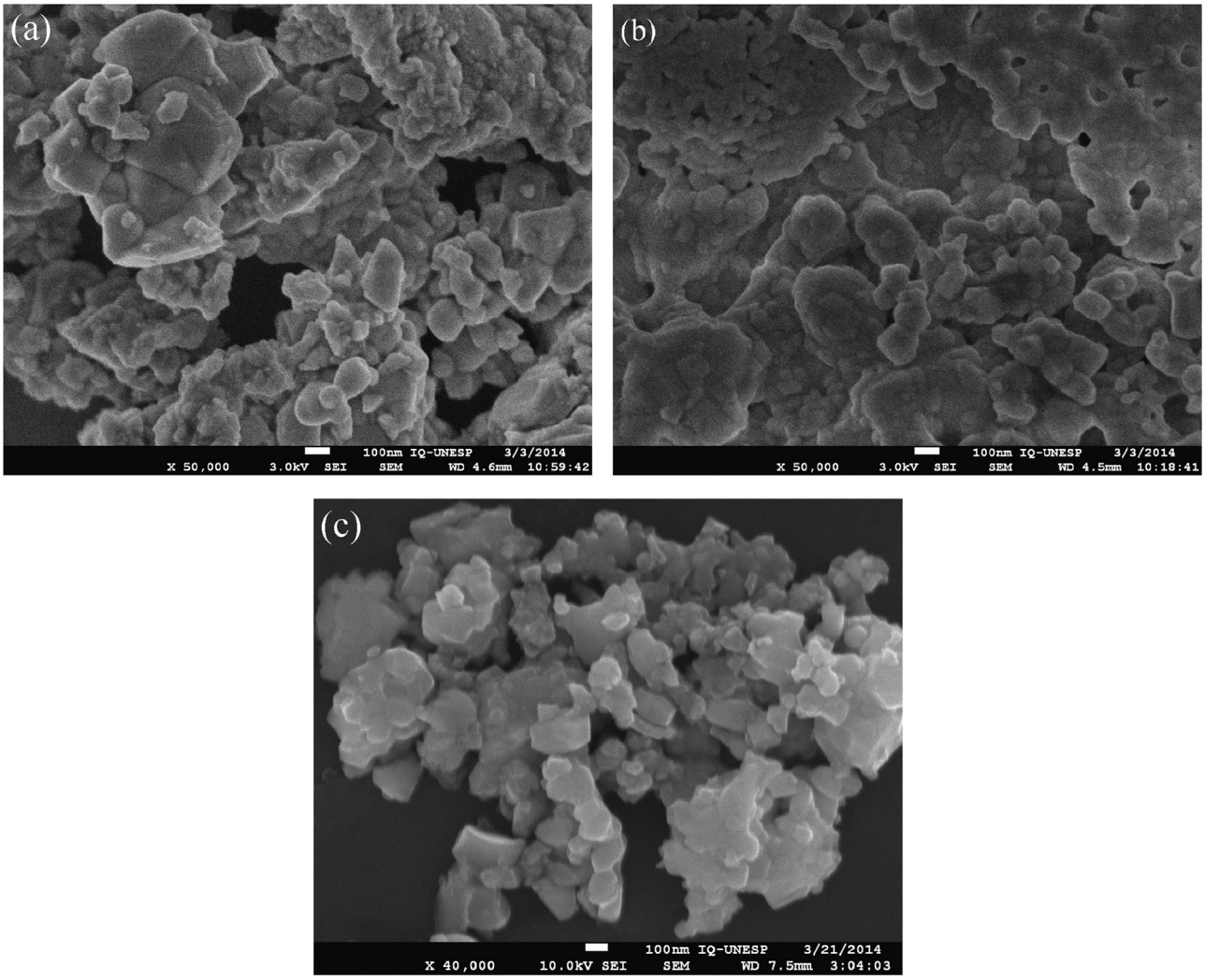

Fig. 4. SEM images of (a) NZF(70–30), (b) BT and (c) NZF(70–30) – BT powders.

microwave synthesis, etc. [17,18]. Recently, auto-combustion synthesis starts to be popular as rapid, cheap and rather simple technique. Ferroelectric component in multiferroic composites, such as barium titanate – $BaTiO_3$ (BT) can be produced using a huge number of various well-known methods. However, to obtain barium titanate through an advanced synthesis method like auto-combustion synthesis is under some difficulties due to lack of the literature data for the preparation of the BT by this method [5].

The aim of this study was to prepare multiferroic composites (Ni–Zn) ferrite–barium titanate from nanopowders obtained by an auto-combustion technique. It was shown that auto-combustion synthesis is very convenient for obtaining the ferrite powder as a pure phase with good properties. To obtain barium titanate by this method is not so simple due to the possible appearance of secondary phases which later may complicate the process of obtaining satisfactory properties of multifferoic composites. A number of different methods were used to characterize obtained powders and ceramic composites in order to fabricate functional multiferroic material with both, ferroelectric and magnetic properties.

2. Material and methods

The multiferroic composite materials, consisting of $Ni_{1-x}Zn_xFe_2O_4$ ($x=0.3$, 0.5, 0.7, denoted as NZF(70–30), NZF(50–50), NZF(30–70) and $BaTiO_3$ (BT), were obtained using the synthesis route shematically presented in Fig. 1.

The raw materials used for the synthesis of nickel zinc ferrite were $Fe(NO_3)_3 \cdot 9H_2O$ (Alfa Aesar, 98.0–101.0%), $Ni(NO_3)_2 \cdot 6H_2O$ (Alfa Aesar, 99.9985%), $Zn(NO_3)_2 \cdot 6H_2O$ (Alfa Aesar, 99%), $C_6H_8O_7 \cdot H_2O$ (Carlo Erba, 99.5–100.5%) and NH_4OH (Lach Ner, 25%). The molar ratio of Fe-ions, Ni+Zn-ions, citric acid was 2:1:1. Metal nitrates and citric acid solution were mixed by dissolving in a minimum amount of deionised water. The pH value of the solution was adjusted to 7 using the ammonia solution. After that the solution was heated and stirred at the temperature of about 90 °C until it converted into a xerogel, which was further heated in a heating calotte at 200 °C when self-propagation reaction was achieved. The formed powder was calcined at 1000 °C/1 h with heating rate 2 °C/min [19].

Starting reagents used for BT synthesis were $Ti(OCH(CH_3)_2)_4$ (TTIP) (Alfa Aesar, 98.0–101.0%), HNO_3, $C_6H_8O_7 \cdot H_2O$ (Carlo

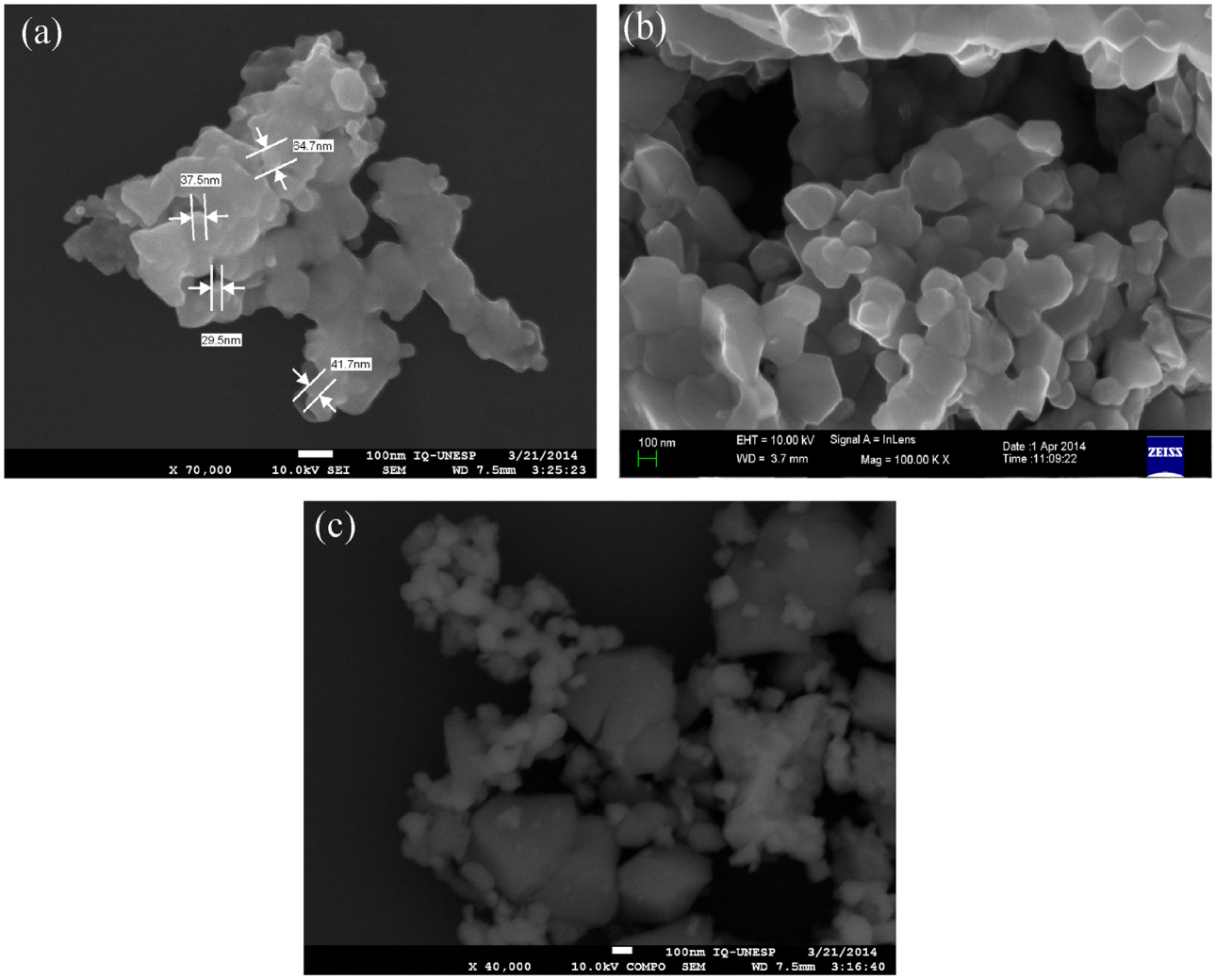

Fig. 5. FEG micrographs of (a) BT, (b) NZF(70–30) and (c) NZF(70–30)–BT powders.

Erba, 99.5–100.5%), $Ba(NO_3)_2$ and NH_4OH (Lach Ner, 25%). Firstly, ammonium hydroxide was added to TTIP solution, with constant cooling. During this process, the yellow precipitate was formed. It was washed with deionized water in a Buchner funnel on a vacuum pump. The obtained residue was dissolved in diluted HNO_3. Solutions of $TiO(NO_3)_2$ and $BaNO_3$ were mixed and citric acid was added as a fuel. pH value of solution was adjusted to 6.6 using NH_4OH. When solution was turned to xerogel, by heating at 90 °C, temperature was raised to 150 °C and self-ignition reaction occurs. It is very fast and exothermic reaction, and gray ash formed during combustion process represents the BT precursor powder. This powder was calcined at 900 °C for 2 h, with a heating rate of 5 °C/min (Electron-UK oven).

Multiferroic composites NZF–BT were prepared by mixing chemically obtained powders of the NZF and BT in the planetary ball mill for 24 h. The mass ratio of NZF and BT was always 1:1 for all obtained samples. Wolfram carbide balls and iso-propanol were used as a milling media. The composites powders were uniaxially pressed at 196 MPa into pellets and sintered at 1200 °C for 2 h.

The phase and crystal structure analysis was carried out by X-ray diffraction technique (Rotate anode Rigaku RINT2000, Experimental conditions: 40 kV, 60 mA. Linear detector D/teX Ultra – Rigaku, Divergence slit: 0, 25, Horizontal aperture slit: 5 mm). Micro-Raman spectra of the synthesized composites were collected at room temperature in the backscattering configuration using a JobinYvon T64000 spectrometer. The 514-nm laser line of a mixed Ar^+/Kr^+ laser was used as an excitation source with an incident laser power 60 mW in order to minimize heating effects. The ceramic composite samples were measured in the range 200–800 cm^{-1}. The FT-IR spectra were recorded with a Bruker Equinox-55 instrument. The morphology of the powders and microstructure of ceramics were examined using scanning electron microscope (SEM Model TESCAN SM-300) and field emission microscope (FE-SEM, JEOL, JSM-7500F). The grain size is determined using ImageJ program. The impedance measurements were performed using an LCR meter (model 9593-01, HIOKI HITESTER). Samples were prepared by coating their polished surfaces with Ag paste to improve the electrical contact. The real and imaginary parts of the complex impedance were measured in the frequency range of 42 Hz to 1 MHz and temperature range of 50–200 °C and referred as the Nyquist plot. Collected data were analyzed using the commercial

software package Z-view. Magnetic measurements of materials were carried out using a superconducting quantum interferometric magnetometer SQUID (Quantum Design).

3. Results and discussion

XRD patterns of NZF(70–30)–BT, NZF(50–50)–BT and NZF(30–70)–BT powders, presented in Fig. 2, shows that nickel zinc ferrite, according to JCPDS files no. 10-0325, and barium titanate phases, according to JCPDS files no. 05-0626, were obtained.

FT-IR spectra of calcined nickel ferrite (NF), zinc ferrite (ZF), BT and NZF(70–30)–BT powders, recorded in the wave number range of 400–4000 cm^{-1} at room temperatures, are presented in Fig. 3. FT-IR spectra of NF and ZF display three bands at 560, 1640 and 3400 cm^{-1}. Strong peak at 560 cm^{-1} corresponds to metal ion-oxygen complexes in the tetrahedral sites. Small peak at 1640 cm^{-1} was assign to the adsorbed water or humidity. The peak at 3400 cm^{-1} corresponds to stretching and banding vibration of O–H bonds [20].

Absorption band near 3500 cm^{-1} can be observed in FTIR spectra of barium titanate. This peak was assigned to the stretching mode of internal OH^- ions [21]. The broad bands at 590–680 cm^{-1} correspond to stretching of Ti–O bond [22].

Fig. 4 shows SEM images of the pure NZF(70–30), BT and composite NZF(70–30)–BT powders. It is possible to notice that the powders indicated the strong agglomeration with small primary particle size (< 100 nm). Small particles produced by chemical synthesis usually tend to form the agglomerates, as it was observed in the investigated case. That problem will be studied more carefully in the future period, having in mind the importance of composite materials properties. The use of attrition milling after calcination could be one of the possible solutions for the agglomeration reduction [23].

The FE-SEM micrographs of the obtained powders (Fig. 5) mostly indicated the rounded shapes of barium titanate particles with primary particle size less than 50 nm. The shape of ferrite particles is pyramidal like. In the composite ferroelectric–ferromagnetic powders obtained by homogenization of individual ferroelectric and ferromagnetic phase, two separate constituents could be clearly noticed, the one with rounded particles that belongs to BT and the other one with pyramidal particle shape that belongs to ferrite, demonstrating that multifferoic composites were obtained with a good dispersion of the nickel–zinc ferrite spinel phase in the BT ferroelectric matrix. The average particle size in the multiferroic composite powders is below 100 nm for BT and 150–300 nm for ferrites.

The XRD difractograms for sintered samples of obtained composites are presented in Fig. 6. The formation of both phases, NZF and BT was detected (JCPDS files no. 10-0325, JCPDS files no. 05-0626). Series of small peaks at 2θ angles of 32.2, 34.1, 37.1, 40.2, 54.9 and 63.1°, according to JCPDS files no. 84-0757, indicated barium ferrite ($BaFe_{12}O_{19}$) as a secondary phase present in the sintered composites.

The relative contribution of the secondary phase, around 8%, was calculated from XRD patterns of ceramics composites, according to the most intensive peak at the 32°. Therefore, it is evident that the amount of the secondary phase is the highest in the case of NZF(70–30)–BT. The appearance of $BaFe_{12}O_{19}$ was noticed in a few published articles, as well [24,25]. Therefore, from the available literature data was concluded that the presence of small amount of this secondary phase cannot significantly affect the magnetic properties of obtained composites. However, for further investigation, an effort will be done to obtain pure phase composites, in order to provide clearer information about influence of secondary phases on the properties of ferroelectric–ferromagnetic composites.

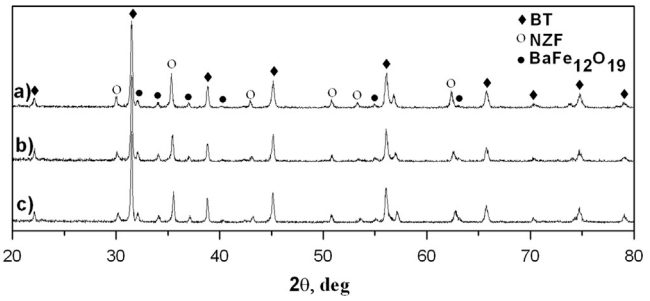

Fig. 6. The XRD patterns of (a) NZF(30–70)–BT, (b) NZF(50–50)–BT and (c) NZF(70–30)–BT ceramics.

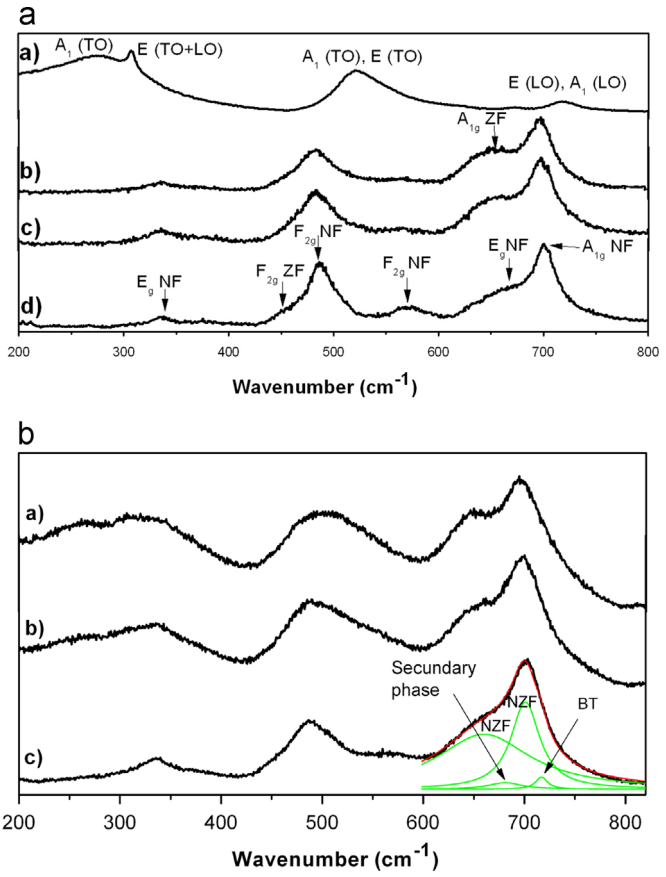

Fig. 7. (a) Raman spectra of (a) BT, (b) NZF(30–70), (c) NZF(50–50), and (d) NZF(70–30) and (b) Raman spectra of composites (a) NZF(30–70)–BT, (b) NZF(50–50)–BT and (c) NZF(70–30) at room temperature.

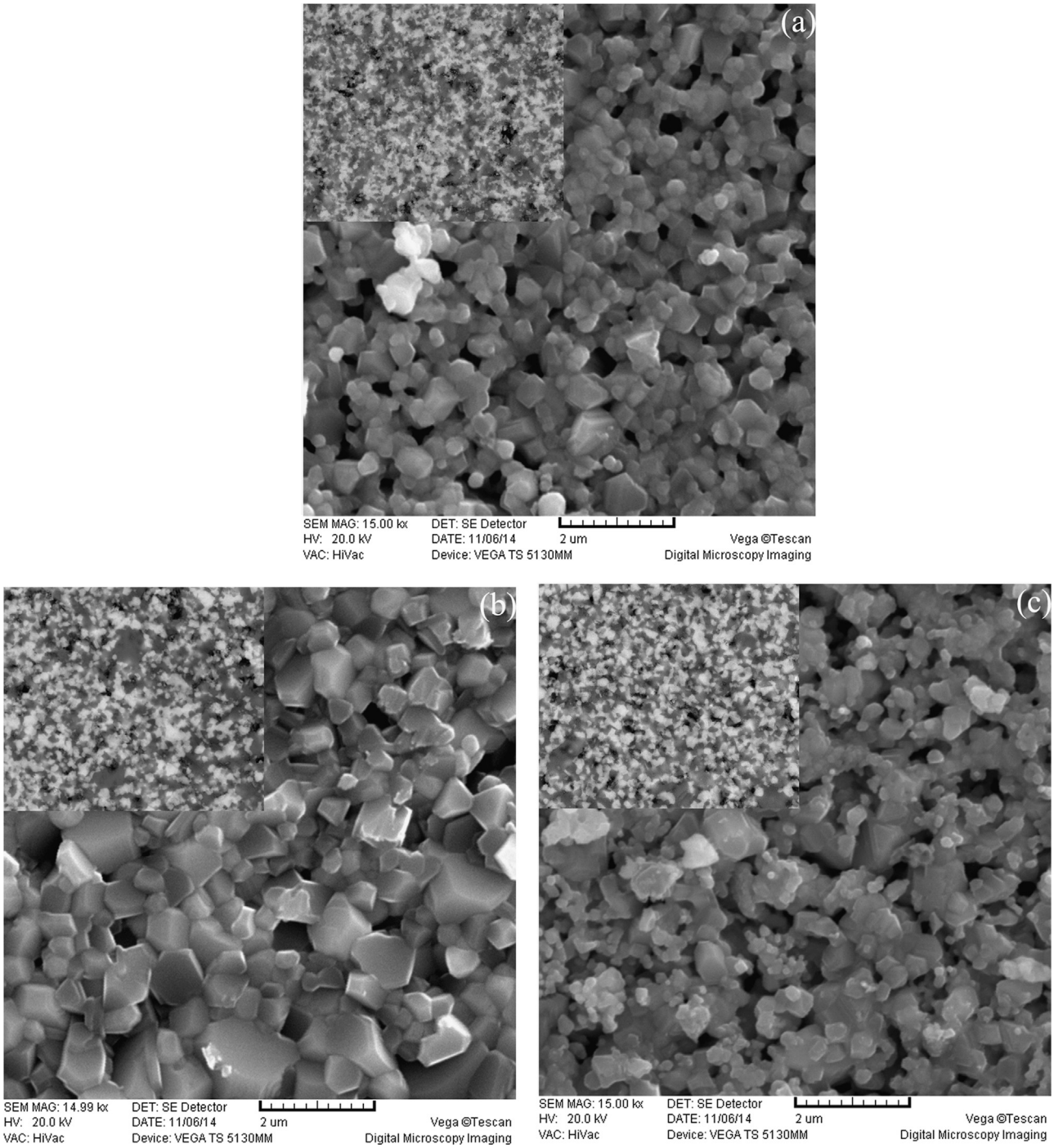

Fig. 8. SEM images of (a) NZF(30–70)–BT, (b) NZF(50–50)–BT, and (c) NZF(70–30)–BT ceramics.

The Raman spectra of $BaTiO_3$ and $Ni_{1-x}ZnFe_2O_4$ ceramics (x=0.3, 0.5 and 0.7) are given in Fig. 7a) for the comparison with obtained composite materials. In the spectra of NZF(70–30) ceramics the most intense Raman modes of nickel ferrite phase are two F_{2g} modes at 482 and 575 cm^{-1}, one E_g mode at 335 cm^{-1} and one A_{1g} mode at 702 cm^{-1} with a shoulder at 666 $cm^{-1}$of E_g symmetry [26,27]. The most prominent modes of the zinc ferrite phase are the F_{2g} mode at 451 cm^{-1} and broad A_{1g} mode at around 647 cm^{-1} of low intensity [28,29]. With increasing content of Zn in the $Ni_{1-x}Zn_xFe_2O_4$ samples, the F_{2g} mode of zinc ferrite becomes more intense and the E_g mode of nickel–ferrite at 660 cm^{-1} shifts to the lower frequency, approaching the frequency of zinc–ferrite A_{1g} mode. The other F_{2g} mode of nickel ferrite phase at 575 cm^{-1} almost disappears in the NZF(30–70) sample.

The Raman spectrum of the $BaTiO_3$ tetragonal phase presented the most prominent Raman modes are a broad band at about 270 cm^{-1} [A_1 (TO)], a sharp peak at ~303 cm^{-1} [E (TO+LO) mode], a mode at 516 cm^{-1}[A_1 (TO), E (TO)] and a mode at around 720 cm^{-1} [E (LO), A_1 (LO)] [30].

The Raman spectra of the sintered composites are presented in Fig. 7b). In the Raman spectra of NZF(70–30)–BT sample, several Raman modes of nickel ferrite suffered changes in the position, intensity and bandwidth. The Raman mode at 482 cm^{-1} is asymmetrically broadened towards higher frequencies, whereas the intensity of 575 cm^{-1} mode decreases. The width of the A_{1g} mode at 702 cm^{-1} increases reflecting the presence of more than two phases. In the fitting range from 600 to 800 cm^{-1} for NZF (70–30)–BT ceramics, it could be seen that this mode is well fitted with three phases, nickel ferrite, BT phase and a secondary phase, $BaFe_{12}O_{19}$ [31,32]. This result is in agreement with previously discussed XRD results.

The noticeable changes were seen in the Raman spectra of the NZF(50–50)–BT and NZF(30–70)–BT samples. In the NZF(50–50)–BT sample, the mode at 335 cm^{-1} of nickel ferrite phase was substantially broadened, whereas the mode of BT phase at around 265 cm^{-1} appeared. The deformation of the nickel ferrite mode at 482 cm^{-1} and its shift to higher frequencies, due to the presence of BT phase, is obvious. With further reduction of nickel ferrite phase in the NZF(30–70)–BT sample, the broad Raman mode at about 500 cm^{-1} is composed of F_{2g} and [A_1 (TO), E (TO)] modes of nickel zinc ferrite and $BaTiO_3$.

SEM images of sintered ceramic samples on the free surface are presented in Fig. 8. Insets of the images are displaying backscattered micrographs, demonstrating the homogenous phase distribution in obtained composites. Grains are nano-sized with different shapes, polygonal grains typical for nickel zinc ferrite, rounded grains characteristic for barium titanate and plate like grains that most likely correspond to the barium ferrite phase. All phases possess similar grain size, around 1 μm. The densities of composites were 5.09 g/cm^3 for NZF (70–30)–BT, 5.28 g/cm^3 for NZF(50–50)–BT, 5.15 g/cm^3 for NZF(30–70)–BT which corresponds to 89.6%, 93.0% and 90.8% of theoretical densities, respectively, showing the increasing trend with Zn content up to NZF(50–50)–BT and then with further increase of Zn the density starts to decrease. Theoretical values of density are 6.01 g/cm^3, 5.35 g/cm^3, 5.36 g/cm^3 and 5.33 g/cm^3 for the pure BT, NZF(70–30), NZF(50–50) and NZF(30–70) phases, respectively. Achieved ceramics densities are rather small due to high agglomeration and this can evidently affect the electrical (dielectric, ferroelectric) properties. This problem can be possibly solved by a treatment in the attrition mill, which may enable the preparation of ceramic composites with improved properties. The FE-SEM microstructure of composites is presented in Fig. 9. It is possible to notice two different phases: ferrites (platelike or pyramidal grains) and barium titanate with more rounded grains. It is important to notice that no reaction between parent components was observed.

The impedance spectroscopy (IS) is important method to study the electrical properties of one material, because it gives the information about resistive and reactive components in the material. IS was used to evaluate the contributions of various components such as grain and grain boundary to the overall electrical properties of NZF–BT ceramics composites. Fig. 10 shows the impedance plots for NZF(70–30)–BT, NZF(50–50)–BT,

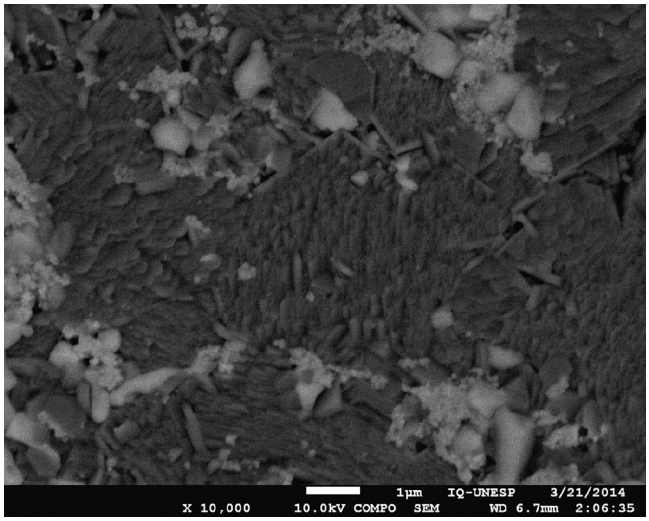

Fig. 9. FEG microstructure of NZF(70–30)–BT composite sintered at 1200 °C for 2 h.

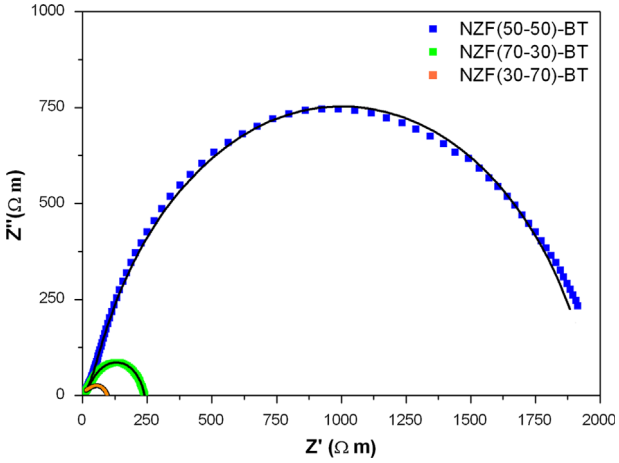

Fig. 10. Complex impedance spectra of all ceramics measured at 200 °C.

Table 1
Grain resistance, grain boundary resistance, total resistance and capacitance for all samples.

Sample	From Z'' to Z'				From Z'' to f	
	T (°C)	R_g (Ω m)	R_{gb} (Ω m)	R_{total} (Ω m)	R_{gb} (Ω m)	C_{gb} (nF/m)
NZF(30–70)–BT	50	155	7113	7268	4326	72.17
	100	117	1296	1413	822	74.45
	150	76	390	466	268	74.13
	200	22	74	96	52	72.12
NZF(50–50)–BT	50	250	54,039	54,289	30,882	109.71
	100	234	9231	9465	6844	135.27
	150	208	6562	6770	5380	160
	200	39	1929	1968	1504	146.24
NZF(70–30)–BT	50	585	36,480	37,065	24,590	99.63
	100	430	16,401	16,831	11,850	94.63
	150	57	492	549	398	85.87
	200	31	207	238	172	78.4

NZF(30–70)–BT ceramics at 200 °C. The impedance spectra were analyzed using commercially available Z-View software. For all samples, a one depressed semicircular arcs is present, indicating the possible overlapping of two arcs that correspond to grain and grain boundary contributions. The Z view software and equivalent circuit consisted of two parallel R-CPE elements connected in series, which were used to evaluate the grain boundary resistivity at low frequencies and grain contribution at high frequencies. The existence of two different phases (ferroelectric and ferromagnetic) in one composite material can make the interpretation of impedance results of these materials rather complicated. The appearance of two semicircular arcs could be also the indication of the presence of two different crystallographic phases. When compared to resistivity values of pure BT and NZF phases [19,33], quite a difference in the resistivity magnitude can be observed. BT, ferroelectric phase, is more resistive in comparison with NZF phase, indicating its dominant effect in the total resistivity of the composite materials. The values of the grain, grain boundary and total electrical resistivity of obtained ceramic composites are presented in Table 1.

With increasing temperature, the resistance of the grain and the grain boundary decreases for all composites (Table 1), as it was expected. Comparing the total resistance at the same temperature, it can be noticed that NZF(50–50)–BT possesses the highest values. With increase of Zn content up to 50% the resistance increases, probably because zinc leads to better structure ordering and results in the reduction of defects. Most likely, oxide ion vacancies $Vo^{\bullet\bullet}$ were formed due to loss of oxygen in the sintering process and present the main conductive species in the obtained ceramics [19].

The temperature dependence of the resistance can be presented by the equation [34]:

$$\sigma = \sigma_0 \exp\left(-\frac{E_a}{k_b T}\right) \quad (1)$$

where E_a, σ_0 and k_b are the activation energy of the carriers for conduction, the pre-exponential factor and the Boltzmann constant, respectively. Arrhenius plots of the grain, σ_g, and grain boundary conductivity, σ_{gb}, for NZF(30–70)–BT, NZF(50–50)–BT and NZF (70–30)–BT ceramics are presented in Fig. 11. The activation energy can be calculated from the slope of the given diagrams. The values of the grain and grain boundary activation energies were: $E_a(g)=0.15$ eV, $E_a(gb)=0.39$ eV for NZF(30–70)–BT, $E_a(g)=0.17$ eV, $E_a(gb)=0.27$ eV for NZF(50–50)–BT and $E_a(g)=0.28$ eV, $E_a(gb)=0.49$ eV for NZF(70–30)–BT. Generally, the activation energies for electron hopping are lower than for hole

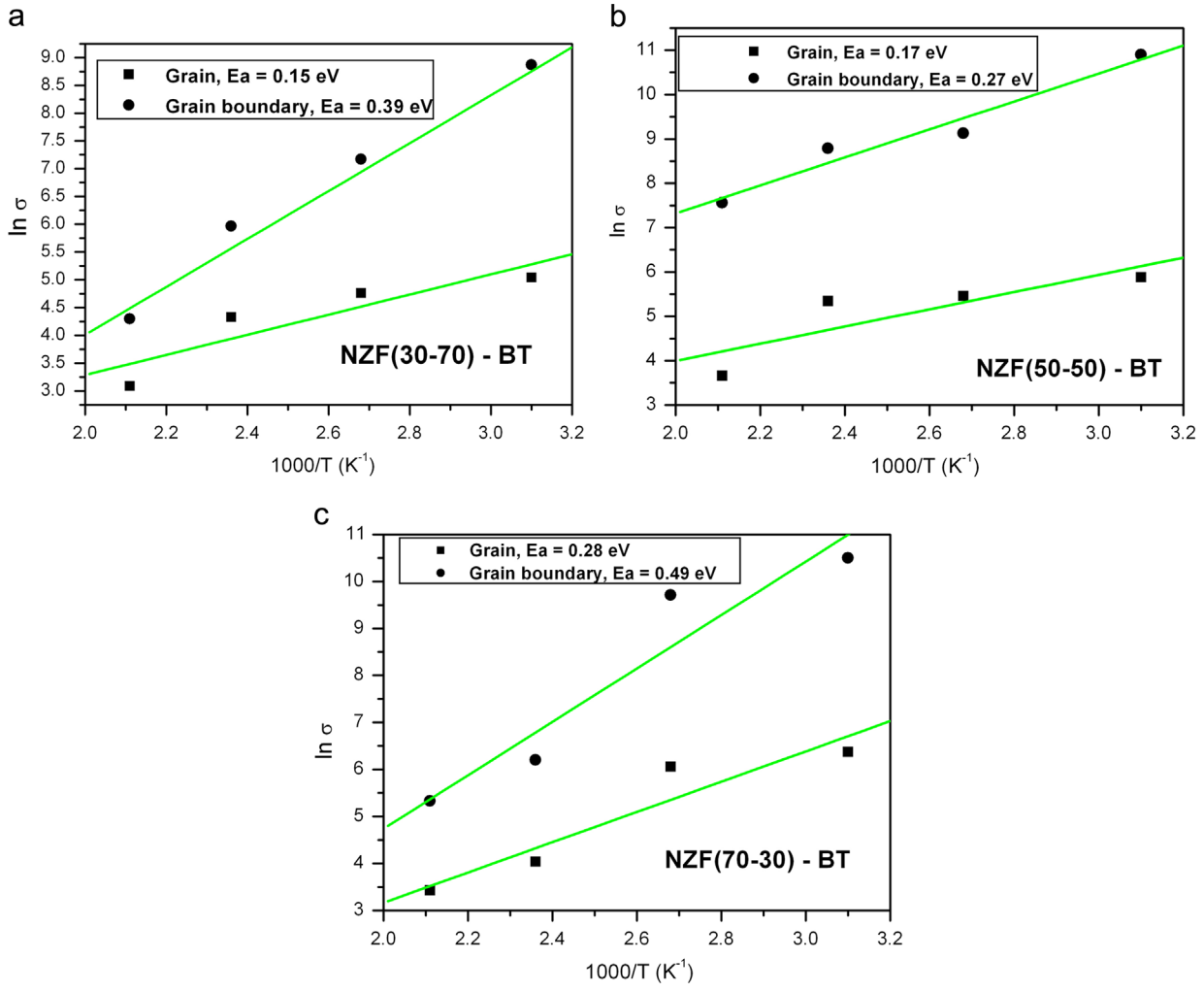

Fig. 11. Arrhenius plots of grain (σ_g) and grain boundary (σ_{gb}) conductivity for all ceramic samples.

hopping. In the polaron conduction, the activation energy of holes is usually used to be greater than 0.2 eV [35]. On this basis, the calculated activation energies indicate that the conduction in obtained materials is a consequence of polaron hopping. The conduction in ferrites, ferroelectrics and its composites can be explained by polaron hopping process among the localized sites. Hopping conduction is favored in ionic lattices in which the same kind of cation is found in two different states [36]. Thus, in the obtained composite materials the hopping of 3d electrons among Fe^{2+} and $Fe^{3}+$ as well as between Ni^{2+} and Ni^{3+} in the ferrite phase and also Ti^{4+} to Ti^{3+} in the ferroelectric phase, could play an important role in the conduction processes. These values for E_a are also in agreement with the results obtained for barium strontium titanate–nickel zinc ferrite composites in the study of other authors [25,37]. The activation energy for the conduction process through the grain boundaries in all measured samples was higher compared to the values of the activation energy for the conduction process through the grains. Therefore, the grain boundary effect can be ascribed as the dominant effect in total conduction of ceramic composites.

Complex modulus plots (M''–M') at the different temperatures for NZF(30–70)–BT, NZF(50–50)–BT, NZF(70–30)–BT are shown in Fig. 12. Values of M'' and M' were calculated from equations $M''=\omega C_o Z'$ and $M'=\omega C_o Z''$, respectively, where C_o is equal to $\varepsilon_o A/h$ and angular frequency ω is equal to $2\pi f$. The complex electric modulus analysis can be used to separate the electrode polarization effect from the grain boundary conduction process and also to determine the conductivity relaxation times [25]. In the presented diagrams two semicircular arcs can be noticed in NZF(70–30)–BT, NZF (50–50)–BT and NZF(30–70)–BT composites, even though, they were not fully resolved in the complex impedance plots. This is also the indication of the presence of different relaxation processes, due to contribution of grain, grain boundary and/or different crystallographic phases.

Complex impedance plots Z''–f for all ceramic composites are presented in Fig. 13. With increasing temperature the positions of peaks shift toward high frequency side, which leads to the conclusion that the dielectric relaxation is thermally activated process [38]. A relative lowering in the magnitude of Z'' with a shift of the peaks towards the higher frequency arises is possibly due to the presence of space charge polarization or accumulation at the grain boundaries [25]. Broadening of the peaks with rise in temperature can be

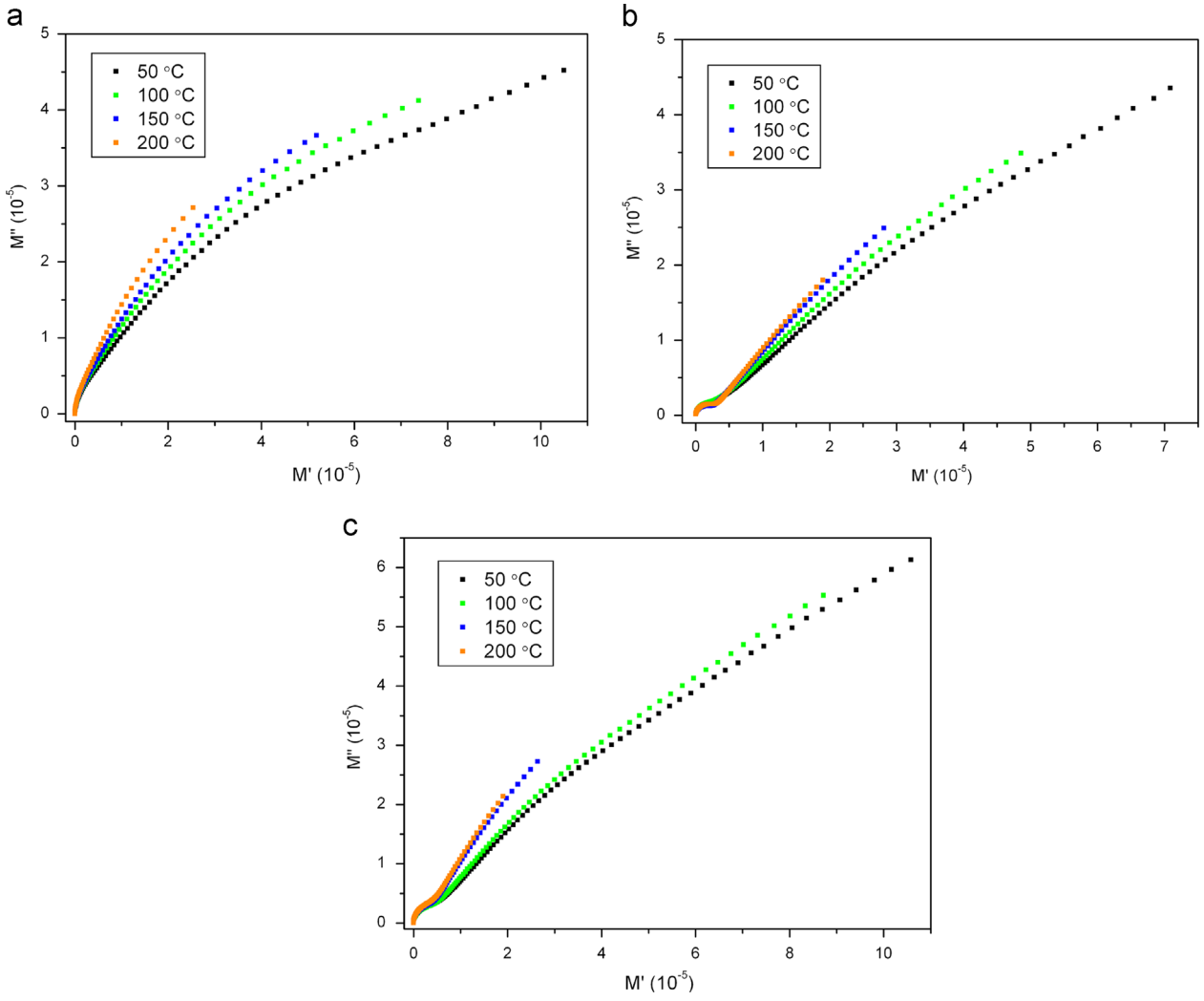

Fig. 12. Modulus complex plots of (a) NZF(30–70)–BT, (b) NZF(50–50)–BT, and (c) NZF(70–30)–BT at different temperatures.

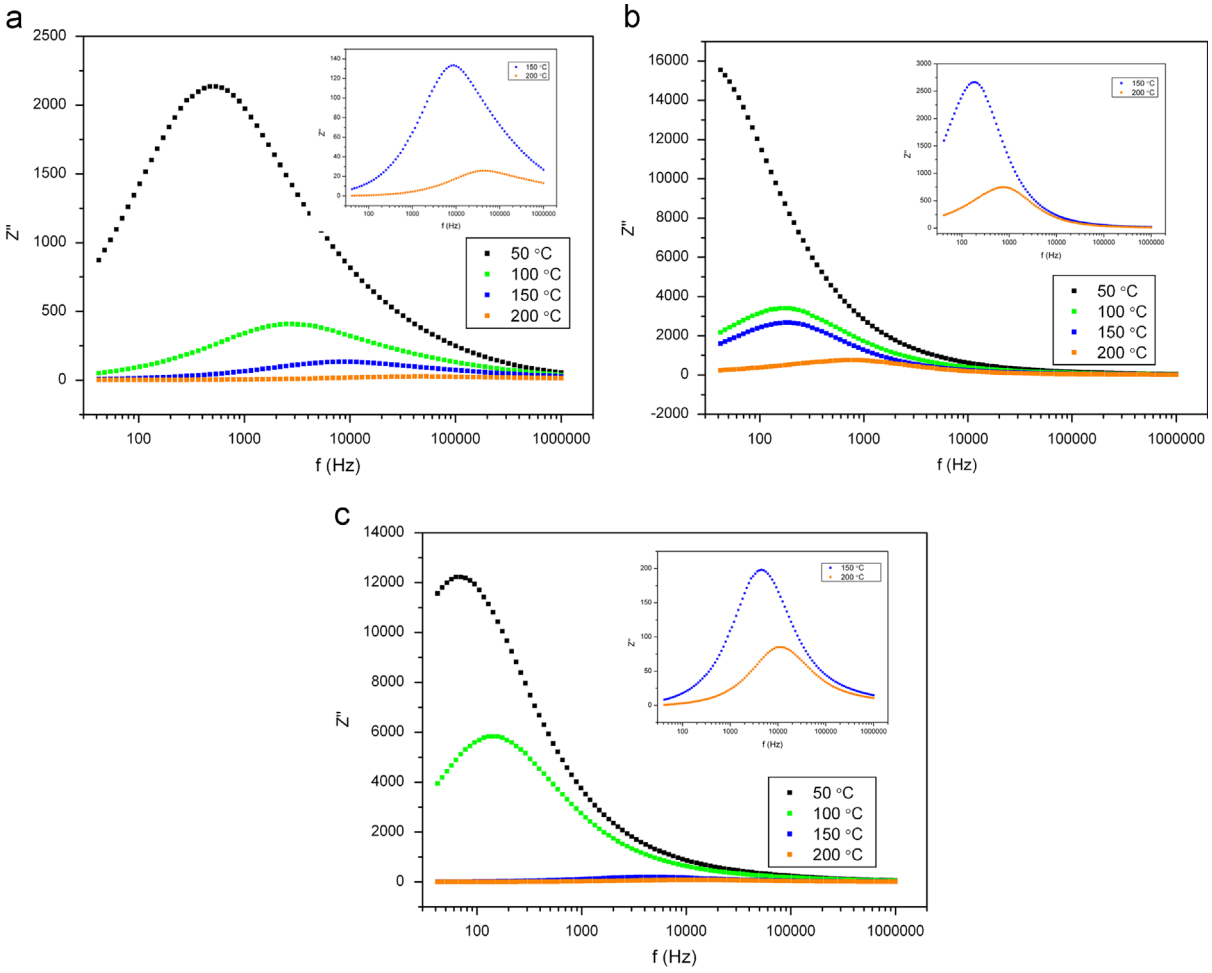

Fig. 13. Frequency dependence of imaginary parts of the impedance spectra (Z'') of (a) NZF(30–70)–BT, (b) NZF(50–50)–BT, and (c) NZF(70–30)–BT at different temperatures.

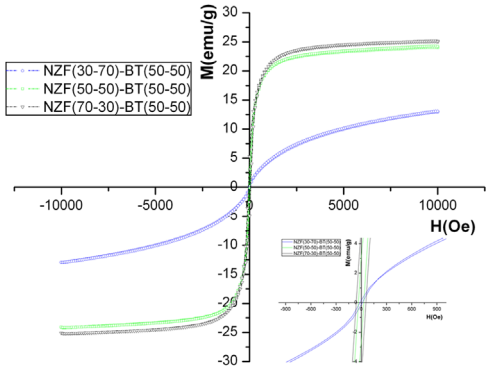

Fig. 14. Magnetic hysteresis loops at room temperature for all composites ceramics.

an indication of the presence of immobile species at low temperature and defects at higher temperatures [39]. The corresponding capacitances and resistivities were calculated from the maximum value of the Z'' peak and associated f_{max} value, using the relationships $C=1/2\pi f_{max}R$, where R is equal to $2Z''_{max}$ [40]. The obtained values for C and R are presented in Table 1. Obtained resistivity data were used for the calculation of activation energies of relaxation processes at the grain boundary and they are in accordance with E_a obtained from the complex impedance analysis.

Table 2
Saturation magnetization moment, saturation fields, residual magnetization and coercive field for $yNi_{1-x}Zn_xFe_2O_4-(1-y)BT$ ($x=0.3$, 0.5, 0.7, $y=0.5$) composite materials.

Sample	M_{sat} (emu/g)	H_{sat} (kOe)	M_r (emu/g)	H_c (Oe)
NZF (70–30)–BT	23.64	2.55	4.31	19.8
NZF (50–50)–BT	22.23	2.05	2.89	25.4
NZF (30–70)–BT	10.42	1.95	0.17	17.6

Magnetization results are presented in Fig. 14 and Table 2. In pure nickel zinc ferrite, with addition of Zn, magnetization increases because the balance between Fe^{3+} ions in tetrahedral and octahedral sites, which is conditioned by migration of the Fe^{3+} ions inter this sites. This leads to the weakening of A–B exchange interaction, causing the increase of magnetization. The change of the magnetic properties with reducing amount of magnetic phase was expected. In composites, a dilution effect exists, which means that BT does cause intimate change in the magnetic properties, leading to the reduction of the magnetic moment [41]. The saturation magnetization and

remnant magnetization have shown a decrease with increasing Zn content, likely due to already mentioned dilution effect. M_s, at first slightly decreases with increase of Zn content up to 0.5 mol% and then significantly decreases with further increase of Zn. In comparison with pure NZF phases, M_s also decreases, due to the presence of non-magnetic barium titanate phase [19]. The fields at which saturation occurs were around 2 kOe for NZF(30–70)–BT and NZF(50–50)–BT and slightly higher for NZF(70–30)–BT. The coercive field, the field required to overcome the defects in the material, was higher for composites in the comparison with pure NZF phases, which can be explained by the fact that the composite possesses a higher anisotropy field than the NZF at the same applied field [35]. The coercive field was the highest for NZF(50–50)–BT ceramic composites.

4. Conclusion

A series of nickel zinc ferrite–barium titanate with general formula $yNi_{1-x}Zn_xFe_2O_4-(1-y)BT$ ($x=0.3$, 0.5, 0.7, $y=0.5$) were successfully prepared by mixing of previously prepared powders of nickel zinc ferrite and barium titanate. The composites materials formation was confirmed by XRD and Raman spectroscopy for powders and ceramics, with small amount of secondary phase. SEM analysis indicated a high level of powder agglomeration and ceramic composites with different shapes grains of around 1 μm. Impedance analysis has shown that for all obtained ceramic samples grain boundary resistance has the highest contribution to the total resistance. The resistance was found to decrease with the increasing temperature for all measured samples, and it can be noticed that NZF(50–50)–BT possesses the highest values of total resistance. The calculated activation energy indicates that the conduction in the composite materials is a consequence of polaron hopping. Results of the magnetic measurements show that the magnetization in the composites ceramics is reduced in comparison with pure nickel zinc ferrite ceramics due to the presence of barium titanate phase. The fields at which saturation occurs were almost the same for all investigated compositions.

Acknowledgments

The authors gratefully acknowledge the financial support of the Ministry of Education, Science and Technological Development of the Republic of Serbia (Project III 45021), COST MP 0904 and IC 1208. Special thanks to Dr. Lavinia Curecheriu from Faculty of Physics, Al.I. Cuza University, Iasi, Romania for magnetic measurements and to Dr. Sonia Zanetti from Institute for Chemistry UNESP, Araraquara, Brazil for FEG microstructure measurements. Also we would like to thank Dr. Zorana Dohcevic-Mitrovic from Institute of Physics, University of Belgrade for useful suggestions about Raman spectroscopy measurements.

References

[1] H. Schmid, Multi-ferroic magnetoelectrics, Ferroelectrics 162 (1994) 317–338.
[2] T. Kimura, T. Goto, H. Shintani, K. Ishizaka, T. Arima, Y. Tokura, Magnetic control of ferroelectric polarization, Nature 426 (2003) 55–58.
[3] N. Hur, S. Park, P.A. Sharma, J.S. Ahn, S. Guha, S.W. Cheong, Electric polarization reversal and memory in a multiferroic material induced by magnetic fields, Nature 429 (2004) 392–395.
[4] L. Mitoseriu, Magnetoelectric phenomena in single-phase and composite systems, Bol. Soc. Esp. Ceram. 44 (3) (2005) 177–184.
[5] M.E. Botello-Zubiate, D. Bueno-Baques, J. de Frutos, L.E. Fuentes, J.A. Matutes-Aquino, Synthesis and magnetoelectric characterization of cobalt ferrite–barium titanate composites using a new pulsed magnetic field method, Integr. Ferroelectr. 83 (2006) 33–40.
[6] C.W. Nan, M.I. Bichurin, S. Dong, D. Viehland, G. Srinivasan, Multiferroic magnetoelectric composites: historical perspective status and future directions, J. Appl. Phys. 103 (2008) 031101.
[7] M.A. Khan, T.P. Comyn, A.J. Bell, Growth and characterization of tetragonal bismuth ferrite–lead titanate thin films, Acta Mater. 56 (2008) 2110–2118.
[8] N. Ikeda, H. Ohsumi, K. Ohwada, K. Ishii, T. Inami, K. Kakurai, Y. Murakami, K. Yoshii, S. Mori, Y. Horibe, H. Kito, Ferroelectricity from iron valance ordering in the charge-frustrated system $LuFe_2O_4$, Nature 436 (2005) 1136–1138.
[9] S.W. Cheong, M. Mostovoy, Multiferroics: a magnetic twist for ferroelectricity, Nat. Mater. 6 (2007) 13–20.
[10] W. Eerenstein, N.D. Mathur, J.F. Scott, Multiferroic and magnetoelectric materials, Nature 442 (2006) 759.
[11] D.B. Litvin, Ferroic classifications extended to ferrotoroidic crystals, Acta Cryst. A 64 (2008) 316–320.
[12] T. Lottermoser, T. Lonkai, U Amann, D. Hohlwein, J. Ihringer, M. Fiebig, Magnetic phase control by an electric field, Nature 430 (2004) 541–544.
[13] B.B. van Aken, T.T. Palstra, A. Filippetti, N.A. Spaldin, The origin of ferroelectricity in magnetoelectric $YMnO_3$, Nat. Mater. 3 (2004) 164–170.
[14] H. Kavas, N. Kasapoglu, A. Baykal, Y. Koseoglu, Characterization of $NiFe_2O_4$ nanoparticles synthesized by various methods, Chem. Pap. 63 (4) (2009) 450–455.
[15] J.V. Boomgaard, R.A.J. Born, A sintered magnetoelectric composite material $BaTiO_3$–Ni(Co, Mn)Fe_2O_4, J. Mater. Sci. 13 (1978) 1538–1548.
[16] N.R. Reddy, E. Rajagopal, K.V. Sivakumar, K.K. Patankar, V.R.K. Murthy, Effect of temperature on the elastic and anelastic behaviour of magneto-ferroelectric composites $Ba_{0.8}Pb_{0.2}TiO_3+Ni_{0.93}Co_{0.02}Mn_{0.05}Fe_{1.95}O_{4-\delta}$ in the ferroelectric rich region, J. Electroceram. 11 (2003) 167–172.
[17] G.R. Amiri, M.H. Yousefi, M.R. Abolhassani, S. Manouchehri, M.H. Keshavarz, S. Fatahian, Magnetic properties and microwave absorption in Ni–Zn and Mn–Zn ferrite nanoparticles synthesized by low-temperature solid-state reaction, J. Magn. Magn. Mater. 323 (2011) 730–734.
[18] D. Chen, R. He, Synthesis of nickel ferrite nanoparticles by sol–gel method, Mater. Res. Bull. 36 (2001) 1369–1377.
[19] A.S. Džunuzović, N.I. Ilić, M.M. Vijatović Petrović, J.D. Bobić, B. Stojadinović, Z. Dohčević-Mitrović, B.D. Stojanović, Structure and properties of Ni–Zn ferrite obtained by auto-combustion method, J. Magn. Magn. Mater. 374 (2015) 245–251.
[20] S. Zahi, Synthesis, permeability and microstructure of the optimal nickel–zinc ferrites by sol–gel route, J. Elctromagn. Anal. Appl. 2 (2010) 56–62.
[21] M.H. Frey, D.A. Payne, Grain-size effect on structure and phase transformations for barium titanate, Phys. Rev. B 54 (1996) 3158–3168.
[22] P.R. Arya, P. Jha, G.N. Subbanna, A.K. Ganguli, Polymeric citrate precursor route to the synthesis of nano-sized barium lead titanates, Mater. Res. Bull. 38 (2003) 617–628.
[23] M.M. Vijatovic Petrovic, J.D. Bobic, A.M. Radojkovic, J. Banys, B.D. Stojanovic, Improvement of barium titanate properties induced by attrition milling, Ceram. Int. 38 (2012) 5347–5354.
[24] L. Mitoseriu, V. Buscaglia, M. Viviani, M.T. Buscaglia, I. Pallecchi, C. Harnagea, A. Testino, V. Trefiletti, P. Nanni, A.S. Siri, $BaTiO_3$–$(Ni_{0.5}Zn_{0.5})Fe_2O_4$ ceramic composites with ferroelectric and magnetic properties, J. Eur. Ceram. Soc. 27 (2007) 4379–4382.
[25] K. Verma, S. Sharma, Impedance spectroscopy and dielectric behavior in barium strontium titanate-nickel zinc ferrite composites, Phys. Status Solidi B 249 (2012) 209–216.

[26] G. Dixit, J.P. Singh, R.C. Sriavastava, H.M. Agrawal, Study of 200 MeV Ag^{15+} ion induced amorphisation in nickel ferrite thin films, Nucl. Instrum. Methods B 269 (2011) 133-139.
[27] A. Ahlawat, V.G. Sathe, V.R. Reddy, A. Gupta, Mossbauer, raman and X-ray diffraction studies of superparamagnetic $NiFe_2O_4$ nanoparticles prepared by sol–gel auto-combustion method, J. Magn. Magn. Mater. 323 (2011) 2049–2054.
[28] A. Ahlawat, V.G. Sathe, Raman study of $NiFe_2O_4$ nanoparticles, bulk and films: effect of laser power, J. Raman Spectrosc. 42 (2011) 1087–1094.
[29] J.P. Singh, G. Dixit, R.C. Srivastava, H.M. Agrawal, Ravi Kumar, Formation of latent tracks and their effect on the structural and magnetic properties of nanosized zinc ferrite, J. Alloy. Compd. 551 (2013) 370–375.
[30] Y. Shiratori, C. Pithan, J. Dornseiffer, R. Waser, Raman scattering studies on nanocrystalline $BaTiO_3$, J. Raman Spectrosc. 38 (2007) 1288–1299.
[31] X. Liu, J. Wang, J. Ding, M.S. Chen, Z.X. Shen, The effects of mechanical activation in synthesizing ultrafine barium ferrite powders from co-precipitated precursors, J. Mater. Chem. 10 (2000) 1745–1749.
[32] J. Kreisel, S. Pignard, H. Vincent, J.P. Senateur, G. Lucazeau, Raman study of $BaFe_{12}O_{19}$ thin films, Appl. Phys. Lett. 73 (1998) 1194.
[33] S. Sharma, K. Shamim, A. Ranjan, R. Rai, P. Kumari, S. Sinha, Impedance and modulus spectroscopy characterization of lead free barium titanate ferroelectric ceramics, Ceram. Int. 41 (2015) 7713–7722.
[34] M. Shah, M. Nadeem, M. Idrees, M. Atif, M.J. Akhtar, Change of conduction mechanism in the impedance of grain boundaries in $Pr_{0.4}Ca_{0.6}MnO_3$, J. Magn. Magn. Mater. 332 (2013) 61–66.
[35] M. Atif, M. Nadeem, Interplay between the ferromagnetic and ferroelectric phases on the magnetic and impendance analysis of $(x)Pb(Zr_{0.52}Ti_{0.48})O_3-(1-x)CoFe_2O_4$ composites, J. Alloy. Compd. 623 (2015) 447–453.
[36] C.E. Ciomaga, A.M. Neagu, M.V. Pop, M Airimioaei, S. Tascu, G. Schileo, C. Galassi, L. Mitoseriu, Feroelectric and dielectric properties of ferrite–ferroelectric ceramic composites, J. Appl. Phys. 113 (2013) 074103.
[37] M.I. Klinger, Two-phase polaron model of conduction in magnetite-like solids, J. Phys. C: Solid State Phys. 8 (1975) 3595.
[38] F Borsa, D.R. Torgeson, S.W Martin, H.K. Patel, Relaxation and fluctuations in glassy fast-ion conductors: wide-frequency-range NMR and conductivity measurements, Phys. Rev. B 46 (1992) 795.
[39] A.K. Behera, N.K. Mohanty, B. Behera, P. Nayak, Impendance properties of $0.7(BiFeO_3)$–$0.3(PbTiO_3)$ composite, Adv. Mater. Lett. 4 (2) (2013) 141–145.
[40] F.D. Morrison, D.C. Sinclair, A.R. West, Characterization of lanthanum doped barium titanate ceramics using impedance spectroscopy, J. Am. Ceram. Soc. 84 (3) (2001) 531–538.
[41] L.P. Curecheriu, M.T. Buscaglia, V. Buscaglia, L. Mitoseriu, P. Postolache, A. Ianculescu, P. Nanni, Functional properties of $BaTiO_3$–$Ni_{0.5}Zn_{0.5}Fe_2O_4$ magnetoelectric ceramics prepared from powders with core–shell structure, J. Appl. Phys. 107 (2010) 104–106.